# Prediction of Radiation From Shielding Enclosures Using Equivalent 3-D High-Frequency Models

Wassim Abdelli, Amin Frikha, Xavier Mininger, Lionel Pichon, Hichem Trabelsi

# Prediction of Radiation from Shielding Enclosures using Equivalent 3D High Frequency Models

Wassim Abdelli[1,2], Amin Frikha[1], Xavier Mininger[1], Lionel Pichon[1], and Hichem Trabelsi[2]

[1]Laboratoire de Génie Electrique de Paris, UMR8507 CNRS, SUPELEC, Université Paris-Sud, Université Pierre et Marie Curie, 11 rue Joliot-Curie, 91192 Gif-sur-Yvette, France

[2]Laboratoire des Circuits et Systèmes Electroniques à Hautes Fréquences, Faculté des Sciences de Tunis, Université Tunis El Manar, Campus universitaire El Manar, 2092 Tunis, Tunisie

**In this paper, an efficient method for the prediction of radiation from shielding enclosures using near-field scan data is presented. An Identification Block allows the location of radiation sources, regardless of their interference. It also allows to find physical models that can be substituted to these sources, giving the same radiation pattern than the one provided by the measurement data taken as reference. Once all the parameters of the physical model are found by an Optimized Genetic Algorithm, the Prediction Block can predict the radiation at all space points in near/far field. This method is applied to the radiation from apertures of electromagnetic shielding enclosures, in order to quantify the disruptive impact of the enclosures, including circuits inside, when it is inserted in a complex environment. Numerical and experimental results are presented to demonstrate the validity and efficiency of the proposed approach.**

***Index Terms*—Shielding enclosures, genetic algorithm, radiated emission prediction, source identification.**

## I. Introduction

TO CONTROL the radiation phenomena and to consider ways for reducing electromagnetic interferences, it is necessary to locate and identify radiation sources, and predict their propagation in space. For this purpose, a common proposed idea consists in characterizing the electromagnetic emissions from a disruptive device on the basis of an equivalent multipolar representation. This provides a behavioral model that accounts for the sources actually present in the device.

Indeed, in many complex systems (inside cars or airplanes), the topology of the circuit becomes very complex; also, the scaling ratio between shielding enclosures, electronic circuits and components within is very important, making a full 3D analysis too heavy for such realistic configurations. The idea consists therefore in modeling the outgoing radiation of the shielding enclosures through all these apertures. The whole enclosure is then considered as a "black box" model, which has a set of identified radiation sources, regardless the circuits inside (Fig. 1). The enclosure is therefore replaced by punctual sources of radiation, which can be inserted directly thereafter into the meshing of complex structures. This allows to avoid meshing the enclosure and all circuits inside.

Identification or prediction models were often applied to radiation from Printed Circuit Board (PCB) in free space [1]-[7], and at low frequency. In some methods, parameters related to the number of dipoles and their positions are predefined in advance [1], [3], [4] and sometimes even manually; this requires a prior thorough knowledge of the circuit architecture, which is not always available. Other models [2] use extra complex processes like "image processing" which is a shape recognition algorithm used to identify the positions and the number of equivalent dipoles; the determination of complex moments is made by the least square method [1]-[4], which needs an accurate knowledge of the phase [1]-[3]. These approaches lead to a parameter identification which is not always optimal; besides the fact that the phase measurement is a cumbersome operation, especially at high frequencies. Also, some methods [1]-[3] produce a high number of equivalent dipoles, which are difficult to use in later integrations. In [5]-[7], tools were developed that give an optimal location of dipoles and do not require the measurement of the phase, but some are associated with a cylindrical cartographies measurement and/or a heavy and complex computation, which can take more than several hours for a single frequency. The model presented by [8] requires the measurement of the electric and magnetic field components, and associates it with the Finite-Difference Time-domain model (FDTD) to predict the evolution of the field.

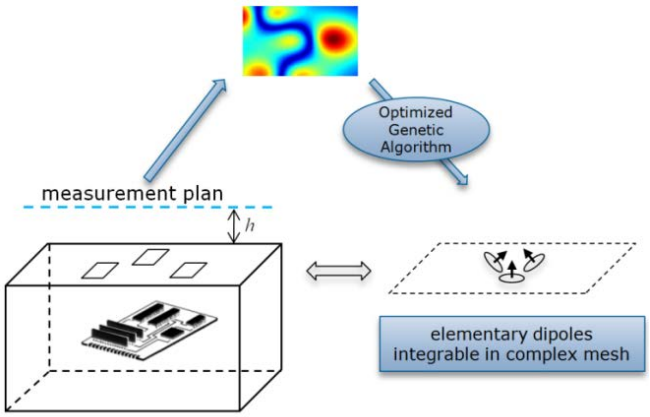


Fig. 1. Basic principle of the method.

This paper presents an efficient method to obtain an

Manuscript received May, 2014. Corresponding author: Wassim Abdelli (e-mail: wassim.abdelli@lgep.supelec.fr).

Digital Object Identifier inserted by IEEE

equivalent 3D model of the shielding enclosures at high frequency. Using an Optimized Genetic Algorithm (OGA) which requires only amplitude measurements of the magnetic field radiated by the device, the optimal parameters of equivalent dipoles are determined: total number of dipoles, positions, orientations, and magnetic moment components. The number of equivalent dipoles obtained is relatively small and proportional to the number of enclosure apertures.

## II. Methodology for Modeling Magnetic Emissions

### A. Equivalent Elementary Magnetic Dipoles

The identification model represents the electronic device to characterize as a set of equivalent elementary sources, which will radiate the same electromagnetic field. These elementary sources are a set of magnetic dipoles (Fig. 2), which are characterized by the following parameters: the total number of dipoles ($N$), positions ($x_{0_i}$ , $y_{0_i}$ , $z_{0_i}$), orientations ($\theta_i$ , $\phi_i$), and magnetic moments ($\overrightarrow{M_i} = M^{\vec{x}}{}_i \overrightarrow{u_x} + M^{\vec{y}}{}_i \overrightarrow{u_y} + M^{\vec{z}}{}_i \overrightarrow{u_z}$), where $i$ is the index number of the dipole.

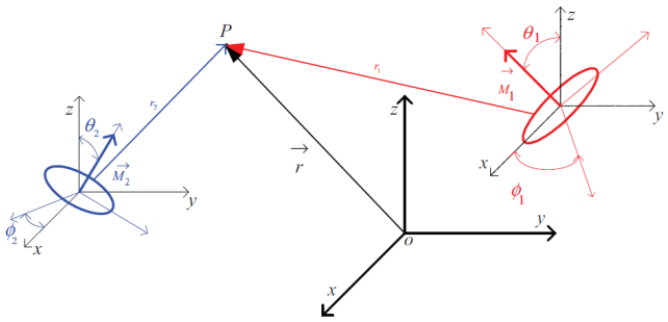


Fig. 2. Elementary magnetic dipoles.

In the Cartesian coordinates, the magnetic field at point $P(x_p , y_p , z_p)$ radiated by an infinitesimal magnetic dipole $i$ placed at ($x_{0_i}$ , $y_{0_i}$ , $z_{0_i}$) with arbitrary orientations can be expressed as [9]:

$$H_i(P) = \begin{bmatrix} H_{x_i} \\ H_{y_i} \\ H_{z_i} \end{bmatrix} = \begin{bmatrix} \Omega^{\vec{x}}_{H_x} & \Omega^{\vec{y}}_{H_x} & \Omega^{\vec{z}}_{H_x} \\ \Omega^{\vec{x}}_{H_y} & \Omega^{\vec{y}}_{H_y} & \Omega^{\vec{z}}_{H_y} \\ \Omega^{\vec{x}}_{H_z} & \Omega^{\vec{y}}_{H_z} & \Omega^{\vec{z}}_{H_z} \end{bmatrix} \begin{bmatrix} M^{\vec{x}}{}_i \\ M^{\vec{y}}{}_i \\ M^{\vec{z}}{}_i \end{bmatrix} \quad (1)$$

with:

$$\Omega^{\vec{x}}_{H_x} = \frac{k^2}{4\pi r_i^3}\left((1-\frac{j}{kr_i}-\frac{1}{(kr_i)^2})r_i^2 - (1-\frac{3j}{kr_i}-\frac{3}{(kr_i)^2})\right)(x_p - x_{0i})^2 e^{-jkr_i}$$

$$\Omega^{\vec{y}}_{H_x} = -\frac{k^2}{4\pi r_i^3}\left(1-\frac{3j}{kr_i}-\frac{3}{(kr_i)^2}\right)(x_p - x_{0i})(y_p - y_{0i})e^{-jkr_i}$$

$$\Omega^{\vec{z}}_{H_x} = -\frac{k^2}{4\pi r_i^3}\left(1-\frac{3j}{kr_i}-\frac{3}{(kr_i)^2}\right)(x_p - x_{0i})(z_p - z_{0i})e^{-jkr_i}$$

where $k$ is the wave number and $r_i$ is the distance from the dipole $i$ to the measurement point $P$, given by:

$$r_i = \sqrt{(x_p - x_{0i})^2 + (y_p - y_{0i})^2 + (z_p - z_{0i})^2} \quad (2)$$

The other coefficients $\Omega$ related to $H_{y_i}$ and $H_{z_i}$ have similar expressions with a coordinate transformation.

From equation (1), the total contribution of magnetic field is obtained at any point $P(x_p , y_p , z_p)$ in space by superposing and adding the emissions of the $N$ elementary dipoles that compose the model:

$$H(P) = \sum_{i=1}^{N} H_i \quad (3)$$

### B. Description of the Methodology

The proposed method supposes that the real source of radiation will be substituted by a set of elementary magnetic dipoles that must determine their unknown parameters. The methodology consists therefore in measuring the cartography of magnetic field components ($H_{x\,meas}$ , $H_{y\,meas}$ , $H_{z\,meas}$) at any height $h$, near the radiating structure; then, the optimal parameters of dipoles are determined using the OGA (Fig. 1). This resolution is based on solving an inverse problem from the near-field cartography. The inverse problem consists in computing a set of unknown source parameters by minimizing an Objective Function ($OF$), which represents the difference between the measured magnetic field and the modeled magnetic field according to the searched parameters.

$$OF_{z_p=h}(X) = \sum_{N_m} \begin{bmatrix} \left(\|H_{x_{meas}}\| - \|H_x(P)\|\right)^2 \\ + \left(\|H_{y_{meas}}\| - \|H_y(P)\|\right)^2 \\ + \left(\|H_{z_{meas}}\| - \|H_z(P)\|\right)^2 \end{bmatrix} \quad (4)$$

with $Nm$ the number of measurement points, $X = \langle N, x_{0_i} , y_{0_i} , z_{0_i} , M^{\vec{x}}{}_i , M^{\vec{y}}{}_i , M^{\vec{z}}{}_i , \theta_i , \phi_i \rangle_{i=1,\ldots,N}$ which represents the vector of unknown parameters that characterize the $N$ dipoles.

The method of OGA is a global stochastic optimization process that is well suited to deals with highly nonlinear problems [10]. It should be noted that the proposed method based on the OGA requires only amplitude measurements of the magnetic field radiated by the device, phase measurements are not necessary.

The position parameters ($x_{0_i}$ , $y_{0_i}$ , $z_{0_i}$) and the moment parameters ($M^{\vec{x}}{}_i , M^{\vec{y}}{}_i , M^{\vec{z}}{}_i$) are deduced directly from the OGA, while the orientation parameters ($\theta_i$ , $\phi_i$) are calculated thereafter from the values of the moments.

$$\phi_i = arctg\left(\frac{M^{\vec{y}}_i}{M^{\vec{x}}_i}\right) \quad (5a)$$

$$\theta_i = arctg\left(\frac{\sqrt{M_i^{\vec{x}\,2} + M_i^{\vec{y}\,2}}}{M_i^{\vec{z}}}\right) \quad (5b)$$

## III. Results and Validation

### A. Numerical results

#### 1) Example 1: square apertures

In Fig. 3, a metallic enclosure is considered. This provides an outgoing magnetic radiation from 3 apertures of a shielding enclosure. This synthetic data provided by a 3D finite element model is used here as measured cartography of the magnetic field.

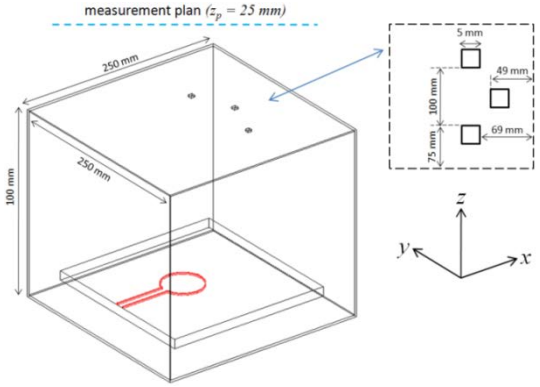


Fig. 3. Shielding enclosure with 3 square apertures on the top face, containing a PCB with a loop-shaped microstrip line.

The source of the magnetic field is a PCB sized 200 mm x 200 mm x 5 mm with a 1 mm wide loop-shaped microstrip line on one side and a ground plane on the other side. The PCB is placed inside a shielding enclosure sized 250 mm x 250 mm x 100 mm, built with a Perfect Electric Conductor material with a thickness of 1 mm. The outgoing magnetic field is radiated from 3 apertures on the top face of enclosure. The apertures are square shaped and sized 5 mm x 5 mm.

Fig. 4 illustrates the results of the model application on the radiation of the shielding enclosure apertures. The radiated magnetic field components are located on a 300 mm x 300 mm scanning plane, situated at 25 mm above the enclosure . From the values of the dipoles (Table I) the cartography predicted on a plane located at 58 mm above the enclosure is deduced and compared to the one obtained with the 3D model.

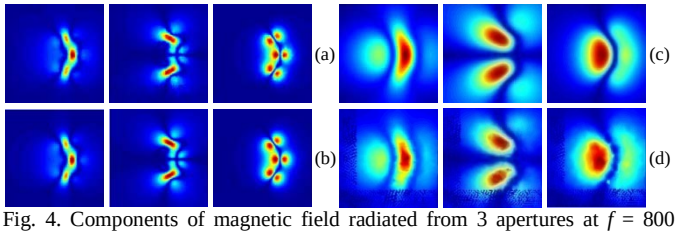


Fig. 4. Components of magnetic field radiated from 3 apertures at $f$ = 800 MHz: (a) magnetic field data at the scanning plane ($z_p$ = 25 mm). (b) modeled magnetic field by the dipoles ($z_p$ = 25 mm). (c) predicted magnetic field by the dipoles ($z_p$ = 58 mm). (d) computed magnetic field with the finite element model ($z_p$ = 58 mm).

Note that only one or two components of magnetic field scanning data is sufficient to perform identification of all dipole parameters and reconstruct the three magnetic field components.

TABLE I
PARAMETERS OF THE EQUIVALENT DIPOLES

| $i$ | $M^{\vec{x}}{}_i$ (Am²) | $M^{\vec{y}}{}_i$ (Am²) | $M^{\vec{z}}{}_i$ (Am²) | $x_{0i}, y_{0i}, z_{0i}$ (mm) | $\theta_i$ ° | $\phi_i$ ° |
|---|---|---|---|---|---|---|
| 1 | 7.60 e-9 | 4.93 e-9 | 0.8 e-12 | 184 , 194 , 0 | 89.99 | 32.9 |
| 2 | 9.32 e-9 | 3.74 e-11 | 0.9 e-11 | 204 , 145 , 0 | 89.94 | 0.01 |
| 3 | 7.67 e-9 | -4.89 e-9 | 0.9 e-12 | 183 , 94 , 0 | 89.99 | -32.4 |

#### 2) Example 2: circular apertures

In this example, the enclosure described in Fig. 3 is used, but with a different apertures configuration on the top face (Fig. 5).

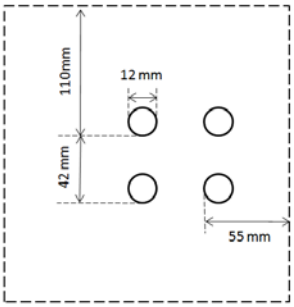


Fig. 5. The top face of a shielding enclosure with 4 circular apertures.

Fig. 6 shows the results of the model application on the radiation of the shielding enclosure apertures. The radiated magnetic field components are measured on a 300 mm x 300 mm scanning plane, situated 20 mm above the enclosure top.

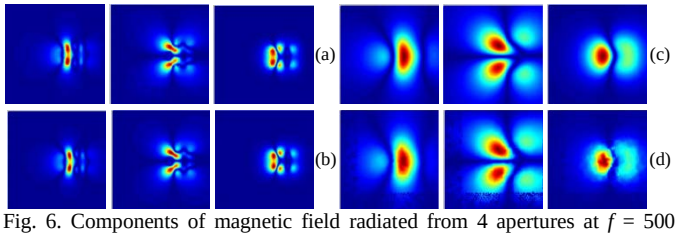


Fig. 6. Components of magnetic field radiated from 4 apertures at $f$ = 500 MHz: (a) magnetic field data at the scanning plane ($z_p$ = 20 mm). (b) modeled magnetic field by the dipoles ($z_p$ = 20 mm). (c) predicted magnetic field by the dipoles ($z_p$ = 50 mm). (d) computed magnetic field with the finite element model ($z_p$ = 50 mm).

TABLE II
PARAMETERS OF THE EQUIVALENT DIPOLES

| $i$ | $M^{\vec{x}}{}_i$ (Am²) | $M^{\vec{y}}{}_i$ (Am²) | $M^{\vec{z}}{}_i$ (Am²) | $x_{0i}, y_{0i}, z_{0i}$ (mm) | $\theta_i$ ° | $\phi_i$ ° |
|---|---|---|---|---|---|---|
| 1 | 3.11 e-8 | 1.25 e-8 | 1.0 e-11 | 187 , 167 , 0 | 89.98 | 21.85 |
| 2 | 1.10 e-8 | 2.66 e-9 | 1.0 e-11 | 227 , 167 , 0 | 89.97 | 13.54 |
| 3 | 3.20 e-8 | -1.32 e-9 | 0.9 e-11 | 187 , 127 , 0 | 89.98 | -22.39 |
| 4 | 1.14 e-8 | -2.71 e-9 | 0.9 e-11 | 227 , 127 , 0 | 89.96 | -13.33 |

Note that the all obtained equivalent dipoles are located in the plane of the apertures (Oxy).

### B. Experimental results

In order to model a realistic case, magnitude cartographies of magnetic field components are required. For this purpose, near-field scanning measurements are performed in a near-field test bench [11] developed in IRSEEM, which consists of

a three-translation-axis robot with a mechanical resolution of 10 $\mu m$ for the three components $(x, y, z)$. A magnetic probe with a surface of 12.5 mm$^2$ is mounted on the robot arm and is connected to a spectrum analyzer as measurement equipment. The probe performs a scan over a planar surface above the device on the XY plane, with a given height $(z_p = h)$. A PC commands the robot and records all results. All the probes (one for $H_x$ and $H_y$, and another for $H_z$) are calibrated with a wire over a ground plane.

The enclosure described in Fig. 7 shows an on-board system, which serves to operate a three-phase motor for a hybrid vehicle. The enclosure contains power electronics, mainly a coil with 8 turns of 23 mm diameter, powered by a 10 dBm signal generator. The enclosure is made of aluminum with a 3 mm thickness.

The outgoing magnetic field is radiated from an insulating gasket which is located between the enclosure and a closure cap screwed. Since the gasket material is non-conducting, it acts as a rectangular radiating slot sized 53.4 mm x 0.54 mm.

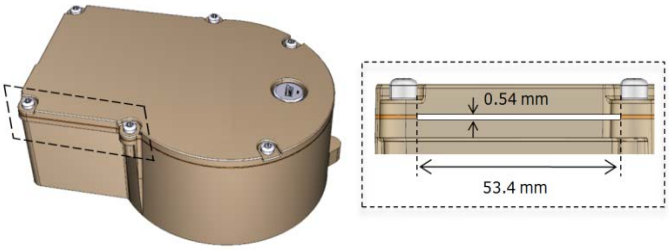


Fig. 7. Geometry of an enclosure with a radiating slot

Fig. 8 illustrates the results of the methodology. The OGA requires here XX individuals, with YY generations. The crossover and mutation probabilities are respectively NN and MM.

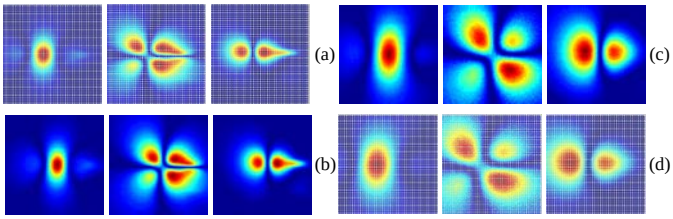


Fig. 8. Components of magnetic field radiated from slot at $f$ = 10 MHz: (a) measured magnetic field data at the scanning plane ($z_p$ = 25 mm). (b) modeled magnetic field by the dipoles ($z_p$ = 25 mm). (c) predicted magnetic field by the dipoles ($z_p$ = 50 mm). (d) measured magnetic field at the scanning plane ($z_p$ = 50 mm).

Fig. 8(a) shows the radiated magnetic field components measured on a 240 mm x 200 mm scanning plane, situated at 25 mm from the slot; the space between sample points is 4 mm in both $x$ and $y$ direction. Fig. 8(b) shows the modeled magnetic field at the same scanning plane, with all parameters determined (Table III). Thanks to the physical model substituting the radiation sources, the Prediction Block can predict the distribution of radiation in all points in near/far field. The plane ($z_p$ = 50 mm) is given as an example (Fig. 8(c)). This prediction is confirmed by measurements made on the same plane ($z_p$ = 50 mm), as shown in Fig. 8(d).

TABLE III
PARAMETERS OF THE EQUIVALENT DIPOLES

| $i$ | $M^{\vec{x}}{}_i$ (Am²) | $M^{\vec{y}}{}_i$ (Am²) | $M^{\vec{z}}{}_i$ (Am²) | $x_{0_i}, y_{0_i}, z_{0_i}$ (mm) | $\theta_i$ ° | $\phi_i$ ° |
|---|---|---|---|---|---|---|
| 1 | 6.14 e-7 | 2.89 e-7 | 0.2 e-10 | 122 , 102 , 0 | 89.99 | 25.17 |
| 2 | 4.11 e-7 | -2.36 e-7 | 0.1e-10 | 144 , 100 , 0 | 89.99 | -29.85 |

## IV. CONCLUSION

A full 3D numerical analysis of complex systems is often too heavy, because of the scaling ratio between shielding enclosures, electronic circuits and components within. In order to avoid these constraints an improved and effective model for identifying and predicting radiated emissions from shielding enclosures has been presented. On the basis of near-field amplitude measurements, the approach provides a behavioral model that accounts for the sources actually present in the device and radiating from apertures. These sources are substituted by a set of magnetic dipoles whose parameters are determined by an Optimized Genetic Algorithm. Numerical and experimental results have shown that the proposed model can predict with a good accuracy at any point the outgoing magnetic radiation from the apertures of the shielding enclosure. Also, it provides equivalent punctual sources of radiation, easily integrable into meshed complex systems.

## REFERENCES

[1] Y. Vives-Gilabert, C. Arcambal, A. Louis, F. de Daran, P. Eudeline, and B. Mazari, "Modeling magnetic radiations of electronic circuits using near-field scanning method," *IEEE Trans. Electromagn. Compat.*, vol. 49, no. 2, 2007, pp. 391-400.

[2] Y. Vives-Gilabert , C. Arcambal , A. Louis , P. Eudeline and B. Mazari, "Modeling magnetic emissions combining image processing and an optimization algorithm," *IEEE Trans. Electromagn. Compat.*, vol. 51, no. 4, pp. 909-918, 2009.

[3] X. Tong, D. W. P. Thomas, A. Nothofer, P. Sewell, and C. Christopoulos, "Modeling electromagnetic emissions from printed circuit boards in closed environments using equivalent dipoles," *IEEE Trans. Electromagn. Compat.*, vol. 52, no. 2, pp. 462–470, May 2010.

[4] B. Essakhi, D. Baudry, O. Maurice, A. Louis, L. Pichon, and B. Mazari, "Characterization of radiated emissions from power electronic devices : synthesis of an equivalent model from near-field measurement," *EPJ Applied Physics Journal*, vol. 38, Issue: 3, 2007, pp. 275-281

[5] L. Beghou, B. Liu, L. Pichon, F. Costa, "Synthesis of Equivalent 3-D Models from Near Field Measurements - Application to the EMC of Power Printed Circuit Boards," *IEEE Trans. on Magn.*, vol. 45, Issue: 3, 2009, pp. 1650-1653.

[6] W. Zhao, B. Wang, E. Liu, H. Park, H. Park, E. Song, and E. Li, "An effective and efficient approach for radiated emission prediction based on amplitude-only near-field measurements," *IEEE Trans. Electromagn. Compat.*, no. 5, 2012. , pp. 1186-1189.

[7] J. Regué, M. Ribo, J. Garrell, and A. Martin, "A genetic algorithm based method for source identification and far-field radiated emissions prediction from near-field measurements for PCB characterization," *IEEE Trans. Electromagn. Compat.*, vol. 43, no. 4, pp. 520–530, 2001.

[8] H. Weng, D. G. Beetner, R. E. DuBroff, "Prediction of Radiated Emissions Using Near-Field Measurements," *IEEE Trans. On Electromagn. Compat.*, vol. 53, 2011, p.891-899.

[9] E. Roubine, J. Bolomey, *Antennes; 1. Introduction Générale*. Paris, France: Masson, 1977.

[10] Z. Michalewicz, "Genetic Algorithms + Data Structures = Evolution Programs," 3rd ed. New York: Springer, 1996.

[11] D. Baudry, "Conception, validation et exploitation d'un dispositif de mesure de champs électromagnétiques proches," Ph.D. dissertation, Univ. Rouen, Rouen, France, 2005.